The multi-omics landscape and clinical relevance of the immunological signature of phagocytosis regulators: Implications for risk classification and frontline therapies in skin cutaneous melanoma

Jiahua Xing
Chinese PLA General Hospital
Ziqi Jia
Peking Union Medical College Hospital
Yan Li
Chinese PLA General Hospital
Yan Han (hanyanhyy10@163.com)
Chinese PLA General Hospital https://orcid.org/0000-0002-2984-6179

Research Article

Keywords: phagocytosis regulators, skin cutaneous melanoma, tumor-associated macrophages, tumor immune cell infiltration, subtype division

Posted Date: May 27th, 2022

DOI: https://doi.org/10.21203/rs.3.rs-1615209/v2

Abstract

Tumor-associated macrophages (TAM) have garnered considerable attention as therapeutic targets. Monoclonal antibody treatment directed against tumor antigens contributes significantly to cancer cell clearance by activating macrophages to phagocytose tumor cells. Compared to other skin malignancies, skin cutaneous melanoma (SKCM) has not yet achieved the expected clinical efficacy and prognosis, owing to its complicated genetic and molecular pathways. Therefore, we choose TAM as an entrance point. This work seeks to thoroughly evaluate the dysregulation and regulatory role of phagocytosis regulators in SKCM and elucidate their regulatory patterns in SKCM. The prognosis-related phagocytosis regulators were subtyped in this work to examine the prognostic differences between subtypes. Then, we screened prognostic factors and constructed phagocytosis-related scoring models for survival prediction using differentially expressed genes (DEGs) between subtypes. Additionally, we investigated alternative treatment options using chemotherapeutic drug response data and clinical cohort treatment data. We first characterize and generalize phagocytosis regulators in SKCM and extensively examine the tumor immune cell infiltration. We created two phagocytosis regulators related system (PRRS) phenotypes and derived PRRS scores using a principal component analysis (PCA) technique. We discovered that subtypes with low PRRS scores had a poor prognosis and decreased immune checkpoint-associated gene expression levels. We observed significant therapeutic and clinical improvements in patients with higher PRRS scores. Our findings imply that the PRRS scoring system can be employed as an independent and robust prognostic biomarker, serving as a critical reference point for developing novel immunotherapeutic methods.

1. Introduction

Currently, we know that phagocytosis is involved in a variety of developmental, homeostatic, and tissue dynamic homeostasis processes inside the organism. It plays a significant role in tumor surveillance [1] [2]; foreign pathogen defense, neutralization and eradication [3]; apoptosis and the clearance of cellular detritus after damage [4] [5] [6] [7] and synaptic pruning [8]. Phagocytes ingest a variety of different particles via a variety of surface receptors and signaling cascades on their cell membranes[9]. Its phagocytosis dysfunction can result in immune system malfunction, aberrant protein aggregation, and developmental abnormalities [9] [10].

In recent years, tumor-associated macrophages (TAM) have gained increased attention as a potential target for tumor therapy. Inflammatory cells are a critical component of cancer's ecological habitat [11] [12], Macrophages, a significant component of leukocyte infiltration, are found in varied amounts throughout all malignancies [13], macrophages are critical inflammatory mediators in tumors. TAM plays a critical function in cancer-related inflammation as a coordinator (CRI) [14]. TAM promotes tumor growth on multiple levels, including promoting genetic instability, the cultivation of cancer stem cells, the establishment of metastasis, and the suppression of adaptive protective immunity. TAM expresses checkpoint activation triggers of T cells and is hence a target for checkpoint blockade immunotherapy. Anti-tumor functional reeducation, M1-like mode; tumor-directed monoclonal antibodies that cause

extracellular death and cancer cell phagocytosis are all examples of macrophage-centered therapeutic methods [15].

Monoclonal antibody therapy targeting tumor antigens mainly eliminates cancer cells by activating macrophages to engulf cancer cells [16] [17] [18] [19]. The methods by which cancer cells evade phagocytosis, on the other hand, are poorly understood. As a “Do not eat me signal”, CD47 is a well-characterized regulator that shields cells from phagocytosis by attaching to macrophages and activating the SIPRA receptor [20] [21]. The CD47-SIPRA axis can inhibit phagocytosis by inhibiting inside-out activation of integrin signaling in macrophages, essential for cancer immunotherapy. Antibody-dependent cellular phagocytosis (ADCP) is a critical step in the interaction between tumor cells and macrophages. The deletion of adipocyte plasma membrane-associated protein (APMAP), a regulator of ADCP susceptibility, synergized with tumor antigen-targeting and CD47-blocking monoclonal antibodies to significantly increase phagocytosis of multiple cancer cell types, including those with ADCP-resistant tumor cells [22].

Skin cutaneous melanoma (SKCM), a malignant tumor of the skin and mucous membranes, is growing every year. In 2021, the United States will accrue more than 100,000 melanoma cases [23]. Its incidence is increasing at a higher rate than all other types of cancer, with roughly 55,000 fatalities globally each year from SKCM [24]. It was the third most prevalent disease among males (684,470 cases) and the fifth most prevalent disease among women in 2019 (672,140 cases) [25]. In comparison to other skin tumors, SKCM has a high late mortality rate, a high recurrence rate, and a high incidence of medication resistance, contributing to its inferior clinical efficacy and prognosis [26] [27]. As an immunogenic tumor, TAM expressing the M2 isoforms are involved in all stages of SKCM formation, represent a significant component of the tumor microenvironment, and are linked with a poor prognosis [28]. TAM is thus a critical and developing site of entry for the treatment of SKCM. Identifying and defining phagocytosis regulators is critical for deciphering the cytophagy pathways in SKCM.

We employed a combination of several databases in this study to distill and summarize phagocytosis regulators discovered in prior research. We used the phagocytosis regulators related system (PRRS) to develop a survival prediction model and assess patient prognosis by fully integrating immune cell infiltration within SKCM. Additionally, we estimated tumor micro-environment (TME) patterns in patients with high and low PRRS subgroups and validated the PRRS scoring method using multiple model validation and clinical validation.

2. Material And Methods

2.1 Phagocytosis regulators regulate macrophage phagocytosis in tumor development

First, we obtain the TCGA database’s relevant expression, phenotype, survival, gene copy, and gene mutation data. The appropriate GEO data is downloaded from the GEO database. Following that, we download the Ensemble database’s human gtf files. We downloaded the set of immune cell-associated genes from Pornpimol Charoentong et al [29]. We downloaded the relationship between immune

infiltrating cells and gene expression from the TIMER database. We organized the data related to this study in Table 1–3.

Table 1
Characteristics of paitients in TCGA-SKCM

Variables	Number of cases
Age(years)	251/206
≤ 60/>60	
Gender	285/172
Male/Female	
Stage	6/77/136/170/23/10/35
0/I/II/III/IV/I or II nos/not reported	
Pathologic T	23/41/77/90/148/78
$T_0/T_1/T_2/T_3/T_4/T_x$	
Pathologic N	226/73/49/56/34/19
$N_0/N_1/N_2/N_3/N_x$/NA	
Pathologic M	407/24/26
M_0/M_1/NA	
OS	235/222
Alive/Dead	
Cluster	335/122
cluster 1/cluster 2	248/209
DEG cluster	5/18/76/164/52
cluster 1/cluster 2	170/182/105
Clark level	
I/II/III/IV/V	
Breslow depth	
>median(high)/≤median(low)/NA	

Table 2
Characteristics of paitients in GSE54467

Variables	Number of cases
Age(years) ≤ 60/>60	47/32
Gender Male/Female	50/29
Stage I/II/III/not reported	29/29/20/1
Event Alive/Dead	27/52

Table 3
Characteristics of paitients in IMvigor210

Variables	Number of cases
Event Dead/Alive	189/109
Response CR/PR/SD/PD	25/43/63/167

Following that, we investigated how phagocytosis regulators affect macrophage phagocytosis. We collected phagocytosis regulatory factors for later analysis from Roarke A Kamber's [30] and Michael S Haney's [22] studies using a 5% false discovery rate (FDR) threshold. We combined them with those from Meghan A Morrissey's [20] study to access the complete phagocytosis regulators set. We calculated macrophage enrichment scores for cancer samples using the R package GSVA, obtained the results, and normalized the data using the scale function. We then calculated the Pearson correlation between macrophage enrichment scores and phagocytosis regulators expression, grouped the top six genes' expression into high and low expression groups using the median as nodes, and examined the Macrophages enrichment scores in the high and low expression groups.

Additionally, we utilized the R package clusterProfiler to conduct functional analysis on phagocytosis regulators and screened them against p-value < 0.05 and q-value < 0.2 to identify critical enrichment pathways.

Then, we investigated abnormal phagocytosis in SKCM. We obtained the relevant gene sets from the Molecular Signatures Database (MSigDB, https://www.gsea-msigdb.org/gsea/msigdb/index.jsp) using

the keyword phagocytosis, which totaled 34 (Supplementary Table 1), and then grouped the samples by age (> 60 vs. ≤60) and stage (III-IV vs. I-II). We performed gene wet enrichment analysis (GSEA) based on the software default thresholds, taking significant results ($P < 0.05$ and FDR < 0.25) for presentation.

2.2 Phagocytosis regulators genes and transcriptional alterations in tumors

First, we investigated transcriptional and genetic changes in phagocytosis regulators in SKCM. We then studied the differences in the expression of phagocytosis regulators between various subgroups of cancer. Then we downloaded the MAF files of TCGA-SKCM mutations and mapped the mutation landscapes of phagocytosis regulators using the R package maftools. Next, we obtained the TCGA-SKCM data on gene-level copy number variation, counted the copy number changes of phagocytosis regulators, and estimated variation frequencies. Additionally, we retrieved the positions of phagocytosis regulators from human chromosomal GTF data and then used the R package RCircos to generate a gene circos map for position display.

The effect of phagocytosis regulators on tumor survival was then investigated. We combined overall survival (OS) data and then utilized univariate Cox regression analysis to identify genes significantly associated with survival ($P < 0.05$), divided the high and low expression subgroups based on the phagocytosis regulators significantly associated with survival, using their median as the node, and then using the R package survival and survminer to plot Kaplan-Meier (KM) curves of gene expression groups, which aims to explore further the correlation between phagocytosis regulators expression and cancer prognosis.

Additionally, we extracted mutational information for phagocytosis regulators, screened genes that were mutated in at least five samples (1 percent of total samples), screened genes that were significantly associated with survival based on mutation ($P < 0.05$) using univariate Cox regression, and then plotted KM curves based on mutation with or without grouping in conjunction with OS for presentation.

2.3 Different modes of phagocytosis regulation in tumors

Firstly, we classified molecular subtypes using phagocytosis regulators. We used the R package ConsensusClusterPlus to perform unsupervised clustering of samples based on the expression matrix of phagocytosis-regulated genes. The algorithm used was kmdist, and the distance was euclidean. We then obtained molecular subtypes of phagocytosis-regulated genes using the PAC algorithm, followed by survival analysis of samples between subtypes and plotting OS-based KM curves. At the same time, we performed principal component analysis (PCA) with the R package factoextra and FactoMineR and then drew PCA scatter plots.

Next, we performed TME engraving among different phagocytosis subtypes. We first performed GSEA of samples between subtypes of phagocytosis-regulated gene molecules using the Hallmark gene set. Then we calculated StromalScore, ImmuneScore, ESTIMATEScore, and TumorPurity of cancer samples in TCGA-SKCM data using R package estimate, and then counted the differences in sample-related scores

between subtypes. We used the R package GSVA to calculate the enrichment scores of 28 immune infiltrating cells in cancer samples, obtained the results, and normalized the data with the scale function. The proportion of immune cells in cancer samples was also calculated using the R package CIBERSORT and the online TIMER database. We further collected immune checkpoint-related genes from the study of Xing Huang [31]. We then counted the expression differences of related genes among different subtypes in the TCGA-SKCM data.

Then, we performed the validation of regulatory mechanisms among different phagocytosis subtypes. We began screening differentially expressed genes (DEGs) between subtypes using the R package limma with $P < 0.05$ and |logFC|>1. Then, we used the R package clusterProfiler to perform functional analysis on DEGs using p-value < 0.05 and q-value < 0.2 criteria to identify significantly enriched pathways. Following that, we performed unsupervised clustering of samples based on the DEG expression matrix using the R package ConsensusClusterPlus, with pam as the algorithm and euclidean as the distance. We obtained molecular subtypes based on DEGs using the PAC algorithm, followed by survival analysis and plotting of samples between subtypes using OS-based KM curves. Then we further examined the expression of phagocytosis-regulated genes among DEG molecular subtypes.

2.4 Phagocytosis regulators related system (PRRS)

Firstly, we performed the construction of a phagocytosis regulators related system (PRRS). We performed bulk univariate Cox regression analysis for DEG of cancer samples combined with OS data. After regression analysis, we screened genes significantly associated with OS ($P < 0.05$) for PCA analysis to obtain principal component 1 and principal component 2, and calculated the score for each sample based on the following formula: $PRRS = \sum |PC1_i + PC2_i|$. Where *i* denotes the sample, *PC1* denotes principal component 1, and *PC2* denotes principal component 2.

To validate the model efficacy, we divided the high and low PRRS groups based on the PRRS of TCGA-SKCM samples with the median as the node, combined with OS data, plotted KM curves, and judged the difference between high and low PRRS groups as significant at $P < 0.05$. We then used the sample PRRS scores as the model prediction results and combined them with survival data to calculate the area under the curve (AUC) of the model at 1, 3, and 5 years values, and then plotted the receiver operating characteristic (ROC) curves. Then, we downloaded the GSE54467 data from the GEO database and then PCA was performed on the genes significantly associated with OS obtained based on TCGA data to obtain PC1 and PC2, and then attained PRRS scores to confirm our model's efficacy once again.

Following that, we verified whether PRRS was associated with tumor prognosis. To determine whether the PRRS score grouping of TCGA data was an independent prognostic factor, we performed a univariate Cox regression analysis with other prognostic factors (age, gender, stage, cluster). Then, we used multivariate Cox regression to examine the overall prognosis of the above five components (including PRRS score grouping) to demonstrate that the PRRS score factor was an independent prognostic factor. Then we combined GSE54467 data by age, gender, and stage to confirm that PRRS score grouping was an

independent predictive predictor. Additionally, we examined the association of PRRS with other clinical features. Moreover, we counted the PRRS differences between subgroups and tested for the significance of the differences.

2.5 Analysis of the molecular mechanisms of different PRRS

First, we calculated the correlation between PRRS and hallmarks enrichment scores to explore the association between PRRS and cancer hallmarks.

Then, we explored the functional differences between different PRRS groupings. We obtained the differential expression ranking of genes based on high and low PRRS groupings using the R package limma, followed by GESA of differential genes using the gseKEGG and gseGO functions of the R package clusterProfiler ($P < 0.05$).

Next, we explored the TME of different PRRS subgroups. We further examined the difference in GSVA calculated enrichment scores of immune infiltrating cells between high and low PRRS subgroups. We also demonstrated differences in the proportion of immune cells in CIBERSORT and TIMER-calculated cancer samples between high and low PRRS subgroups.

In addition, we explored the differences in genomic alterations across different PRRS subgroups. We used Masked Copy Number Segment data of TCGA SKCM samples to analyze copy number variations (CNV) changes between high and low PRRS groupings online by GenePattern GISTIC 2.0(https://cloud.genepattern.org/gp/p ages/index.jsf). Then, we visualized them using the R package maftools. Moreover, we used the MAF files of TCGA-SKCM mutations, combined with the high and low PRRS groupings, and we utilized the R package maftools to plot the mutation landscapes of the samples between the groupings.

2.6 Potential treatment strategies for PRRS

First, we performed chemotherapy drug resistance prediction. We used the R package pRRophetic to predict the response of samples to 138 drugs to obtain the predicted value of IC_{50}. We then counted the differences in IC_{50} of samples in high and low PRRS groups. Six drugs with significant differences ($P < 0.05$) were selected for presentation after multiple corrections with Bonferroni methods.

In addition, we also performed an exploration of immunotherapy response. We downloaded IMvigor210 bladder cancer data using the R package IMvigor210CoreBiologies. We then performed PCA based on genes significantly associated with OS attained from TCGA to obtain PC1 and PC2, which in turn yielded PRRS scores, divided high and low PRRS score subgroups using median as the node, plotted KM curves for high and low PRRS score subgroups, and counted the differences of PRRS scores of different response groups.

2.7 Validation of expression-based regulators of survival significantly associated with phagocytosis

We used the following cell lines to validate critical genes in SKCM and normal skin tissues. A375 human melanoma cell line (American Type Culture Collection, American), SK-MEL-28 cell line (National Infrastructure of Cell Line Resource, China), human immortalized keratin-forming cell line (Hacat), and human melanocyte line (PIG1) (Shanghai Guandao Biological Engineering Company, China). All cells were cultured in RPMI-1640 culture medium + 10% fetal bovine serum with the surrounding environment maintained at 37°C and 5% CO_2.

Then, we further validated the collected specimens of 15 pairs of SKCM and normal skin tissues. All experimental components were approved by the Human Research Ethics Committee of the General Hospital of the Chinese People's Liberation Army (Chinese PLA General Hospital), and the patients had signed an informed consent form. We used a standard qRT-PCR method to detect the relative expression of nine essential genes [32]. All primers we used were synthesized by Huada Corporation (Beijing, China). In addition, we validated the expression of crucial genes in normal skin tissues and SKCM in the HPA database (https://www.proteinatlas.org/) and further validated our findings by semi-quantitative analysis.

3. Result

3.1 Phagocytosis regulators regulate macrophage phagocytosis in tumor development

Figure 1A depicts the study's flowchart, whereas Fig. 1B depicts the evolution of TAM in the tumor microenvironment and its mechanism of action schematically. We identified 271 phagocytosis regulatory factors in the linked literature, 260 of which included information on their expression. Then we calculated the Pearson correlation coefficients and *P*-values for the 260 phagocytosis regulators and macrophage enrichment scores (Supplementary Table 2), and we used the top six to generate scatter plots. The correlations between the genes shown in the plots and macrophages were larger than 0.8 and $P < 0.01$ (Fig. 2A-F). We further classified the top six genes into high and low expression groups based on their median expression levels, and the results indicated that the macrophage enrichment scores for all genes in the high expression group were significantly higher than those in the low expression group, which was consistent with the correlation results (Fig. 2G-L).

Then, we ran a functional enrichment analysis on genes controlled by phagocytosis. Among these, the examination of GO enrichment was subdivided into three sections: biological process (BP), cellular component (CC), and molecular function (MF). The pathways enriched by BP are primarily immune response-activating cell surface receptor signaling pathways, the pathways enriched by CC are primarily mitochondrial inner membrane pathways, the pathways enriched by MF are primarily transcription coactivator activity pathways, and the pathways enriched by KEGG are primarily thermogenesis pathways, among others (Fig. 2M-P).

To further investigate the aberrant phagocytosis in tumors, we examined the functional enrichment of age grouping (> 60 vs. ≤60) and stage (III-IV vs. I-II) of cancer samples in the set of 34 phagocytosis-

related genes. The results showed that we enriched 5 gene sets in the > 60 groupings for the age grouping, and then we enriched 29 gene sets in the ≤ 60 groupings, but none reached significant levels. While for the stage grouping, we enriched 22 gene sets in III-IV, which reached significant levels with three pathways (Fig. 2Q-S).

3.2 Phagocytosis regulators genes and transcriptional alterations in tumors

We then evaluated differences in the expression of phagocytosis regulatory variables between age, gender, pathologic M, pathologic N, pathologic T, tumor stage, Breslow depth, and Clark level subgroups in cancer samples. The findings revealed that 41 genes were differentially expressed in the age grouping, 19 genes in the gender grouping, 6 genes in the pathologic M grouping, 25 genes in the pathologic N grouping, 109 genes in the pathologic T grouping, 104 genes in the tumor stage subgroup, 131 genes in the Breslow depth subgroup, and 63 genes in the Clark level subgroup (Fig. 3A-H). Due to many phagocytosis regulators, the significant results were tabulated, and we included the details in Supplementary Table 3.

We mapped the mutation profiles of phagocytosis regulators based on the MAF files for TCGA-SKCM mutations. Due to the large number of genes, only the top 20 were displayed, and the results indicated that the mutation rate of the top 20 phagocytosis regulating factors was 66.17% in SKCM samples, with ZDBF2 having the greatest mutation rate, followed by HDAC9 (Fig. 3I). We calculated the copy number changes of phagocytosis regulators using the TCGA-SKCM gene-level copy number data. The top 30 genes were displayed since there were more genes, among which RRAGA had the greatest frequency of deletion and PTEN had the second highest (Fig. 3J). Additionally, we determined the frequency of copy number alterations in the top 30 phagocytosis regulators (Fig. 3K) and plotted the locations of all phagocytosis regulators on each chromosome (Fig. 3L).

We examined the influence of phagocytosis regulators' expression on survival using OS data. Due to a large number of genes, we first used univariate Cox regression to identify those significantly associated with survival. The results indicated that the expression of 84 of 260 phagocytosis regulators was significantly associated with prognosis, with 13 genes having HR > 1 and the remaining 71 genes having HR < 1, as shown in Supplementary Table 4. Then the nine genes with the lowest *P*-value are listed. And then, we presented the KM curves of these nine genes (Fig. 4A-I). We used OS data to investigate the influence of phagocytosis regulator mutations on survival. Due to many genes, we first screened for genes associated with survival using univariate Cox regression. The results indicated that 126 genes had mutations in at least five samples, of which 7 genes had mutations associated with prognosis, with 4 genes having HR > 1 and the remaining 3 genes having HR < 1, as shown in Supplementary Table 5. Following that, we created the KM curves for these seven genes (Fig. 4J-P).

3.3 Different modes of phagocytosis regulation in tumors

We performed unsupervised clustering on phagocytosis regulators' expression matrix samples (Fig. 5A-C) and identified two subtypes with significantly different KM curves (Fig. 5D). The survival curves of cluster

1 samples decreased significantly faster than those of cluster 2, while PCA scatter plots revealed a clear distinction between the two subtypes (Fig. 5E). Additionally, there were significant differences in the expression of phagocytosis regulators between the two subtypes (Fig. 5F).

We then etched the TME between distinct phagocytosis subtypes. We first performed an enrichment analysis of hallmark pathways within samples between subtypes using the MSigDB database and found that 37 out of 50 pathways had significant differences, including HALLMARK_TNFA_SIGNALING_VIA_NFKB and HALLMARK_TGF_BETA_SIGN ALING, which were all significantly different between the two subtypes (Fig. 5G). Additionally, we generated the StromalScore, ImmuneScore, ESTIMATEScore, and TumorPurity scores for cancer samples and quantified the differences in sample-related scores between subtypes. StromalScore, ImmuneScore, and ESTIMATEScore scores were considerably higher in cluster 2 samples than in cluster 1, although TumorPurity scores were significantly higher in cluster 1 samples than in cluster 2 (Fig. 5H-K). The enrichment scores of 28 immune infiltrating cells in cancer samples were then calculated. The results indicated that all immune infiltrating cells were considerably different between the two subtypes, with activated B cells, activated $CD4^+$ T cells, and activated $CD8^+$ T cells scoring significantly higher in cluster 2 than in cluster 1 (Fig. 5L). Additionally, we determined the fraction of immune cells in cancer samples using the R package CIBERSORT and the online TIMER database. We demonstrated the corresponding box plots in Supplementary Fig. 1A-B. Moreover, we compared the expression of immunological checkpoints between subtypes; the results demonstrated that 43 of 45 immune checkpoints exhibit differential expression, with CD274, CTLA4, PDCD1, and LAG3 being considerably overexpressed in cluster 2 (Fig. 5M).

Then, we validated the regulatory mechanisms underlying distinct phagocytosis isoforms. Furthermore, we utilized all protein-coding genes and screened for DEGs between isoforms, then identified 661 DEGs based on threshold values. On DEGs, we performed functional enrichment analysis. The GO enrichment analysis was divided into three sections: BP enrichment pathways were primarily concerned with T cell activation, CC enrichment pathways were primarily concerned with the external side of the plasma membrane, MF enrichment pathways were primarily concerned with cytokine receptor binding, and KEGG enrichment pathways were primarily concerned with cytokine-cytokine receptor interaction (Fig. 6A-D). We then performed unsupervised clustering on the samples using the DEGs' expression matrix. We obtained two isoforms with significant differences in the KM curves of the samples between the isoforms and significant differences in the expression of the DEGs between the two isoforms (Fig. 6E-F). The expression of phagocytosis regulators was then compared between differential subtypes, and the results indicated that the expression of several phagocytosis regulators varied between differential gene expression subtypes (Fig. 6G).

3.4 Phagocytosis regulators related system (PRRS)

We first performed the construction of PRRS. We screened 582 survival-related DEGs using univariate Cox regression based on DEGs in TCGA data, then performed PCA on these 582 genes to obtain PC1 and PC2

for summation, attained PRRS scores, and then divided them into high and low PRRS groups with the median. The difference in KM curves between the two groups was significant. And then, we used the sample risk score as the model prediction result and combined it with the survival data to calculate the AUC of the model. The AUCs of 1, 3, and 5 years were greater than 0.6, indicating good model efficacy (Fig. 7A-E). We validated the model's efficacy in GSE54467. Then we performed PCA based on the expression matrix of survival-related DEGs in GSE54467, attaining PC1 and PC2 and calculating their sum to obtain the PRRS. We utilized the median as the division to obtain the high and low PRRS groups, respectively. The KM curves of the two groups were significantly different, and the AUC values based on the time ROC curves were all greater than 0.6 (Fig. 7F-J).

We further examined the independent prognostic effect of PRRS subgroups using TCGA data. The results showed that the PRRS subgroup, age subgroup, and stage subgroup had better prognostic efficacy and were independent of each other (Fig. 8A-B). Similarly, we combined the age, gender, and stage to verify whether the PRRS score subgroup was an independent prognostic factor in the GSE54467 data. The results demonstrated that the PRRS score subgroups had better prognostic efficacy and were relatively independent (Fig. 8C-D).

Then, we further counted the PRRS differences in age, gender, pathologic M, pathologic N, pathologic T, tumor stage, Breslow depth, Clark level, and molecular subtype groupings. The results demonstrated that the PRRS score of pathologic T gradually decreased with increasing grade; the PRRS score of patients with Clark level of IV-V was significantly lower, and the PRRS score of patients with tumor stage of stage II was significantly lower than that of stage I; the PRRS score of patients with cluster 2 in subtype classification was higher (Fig. 8E).

3.5 Analysis of the molecular mechanisms of different PRRS

We further examined the correlation between PRRS and cancer hallmarks enrichment scores, and the results showed that most pathways were significantly correlated with PRRS, especially HALLMARK TNFA SIGNALING VIA NFKB, HALLMARK APOPTOSIS were significantly positively correlated with PRRS, while HALLMARK DNA REPAIR, HALLMARK MYC TARGETS V2 were significantly and negatively correlated with PRRS (Fig. 9A).

Then, we further performed GESA-based GO and KEGG enrichment analysis based on PRRS grouping. For GO enrichment results, the main enrichment pathways were activation of innate immune response, adaptive immune response, and so on. Additionally, for KEGG enrichment results, the main enrichment pathways are cytokine-cytokine receptor interaction, endocytosis, and so on (Fig. 9B-C).

Following that, we inscribed the TME for the different PRRS groupings. The results indicated that StromalScore, ImmuneScore, and ESTIMATEScore were significantly higher in samples with a high PRRS than in samples with a low PRRS. However, TumorPurity was the inverse (Fig. 9D-G). And then, we counted the enrichment scores of 28 immune infiltrating cells between different PRRS groups. The results indicated a statistically significant difference in the number of immune infiltrating cells in the different

PRRS groups. We concluded that all immune infiltrating cell enrichment scores were significantly greater in high PRRS samples than in low PRRS samples (Fig. 9H). Additionally, we evaluated the differences in immune infiltrating cell proportions between high and low PRRS subgroups using CIBERSORT and online TIMER data. We demonstrated the corresponding box plots in the Supplementary Fig. 2A-B.

Furthermore, we investigated the differences in genomic changes between PRRS subgroups. We calculated the frequency of CNV changes between PRRS subgroups and found that CNV changes were considerably lower in high PRRS samples than in low PRRS samples (Fig. 9I-K). Additionally, we counted the differences in CNV between genes in the PRRS subgroups and found 5202 genes with substantial CNV differences between the two groups. We also evaluated gene mutations between PRRS groupings and found that the mutation rate was slightly greater in high PRRS samples than in low PRRS samples (Fig. 9L-M). We further counted the genes that had significantly different mutations between the two groups of samples. The findings indicated that 325 genes had significantly different mutations between the two groups, as shown in Supplementary Table 5.

3.6 Potential treatment strategies for PRRS

We predicted the reaction of samples in the high and low PRRS groups to 138 medications (Supplementary Table 6). We then displayed box plots to demonstrate the six with both substantial differences and common medications. The results indicated that the high PRRS samples were more medication resistant (Fig. 10A-F).

Additionally, we collected IMvigor210 bladder cancer data and generated sample PRRS scores based on gene expression data within the model. The KM curves indicated no significant differences between the high and low PRRS groups. However, PRRS scores were considerably higher in complete response (CR) samples than in partial response (PR) or progressive disease (PD) samples, implying that PRRS scores may be related with immunotherapy response (Fig. 10G-K). Moreover, the endogenous processes of SKCM and their influence on the antitumor immune response are summarized in Fig. 10L.

3.7 Validation of expression-based regulators of survival significantly associated with phagocytosis

We downloaded immunohistochemical images of phagocytosis regulators based on the expression of significant survival-related (ACTR3, AXL, BIN2, CD38, CIITA, DOCK2, FCGR2A, FCRL3) from the Human Protein Atlas database. The expression levels of these proteins in normal skin and SKCM were confirmed by semi-quantitative analysis. We organized the immunohistochemical maps of the complete field of view in Supplementary Fig. 3. We then validated the expression levels of these 9 significantly related phagocytosis regulators based on expression by qRT-PCR in human tissues and cell lines. The primer sequences we used are shown in Supplementary Table 7. The results showed that ACTR3, AXL, CIITA, DOCK2, FCGR2A, FCRL3 were up-regulated in SKCM, and BIN2, CD38, FCGR1B were down-regulated in SKCM (Fig. 11A-I)

4. Discussion

Despite substantial breakthroughs in biological cellular immunotherapy and immune checkpoint blocking (ICB) therapy for SKCM, many SKCM remain immune resistant. The 5-year survival rate for stage IV SKCM remains less than 19 percent [33]. In recent years, immune cell infiltration has been identified as a robust and predictive biomarker of prognosis in SKCM [34] [35]. Despite extensive clinical trial data demonstrating immunotherapy's efficacy in advanced metastatic SKCM, 35–60% of patients developed resistance to PD-1 blocking immunotherapy in recent years [36] [37] [38]. Between 40% and 65% of patients develop mild medication resistance, whereas 43% develop acquired drug resistance [37]. In recent years, many clinical trials have focused on exploring the ICB in combination with targeted agents (BRAF mutation inhibitors, MEK inhibitors, ALK inhibitors) and immune factor inhibitors (CD40, CD137, CD134, CD357) for the treatment of advanced SKCM, showing some synergistic effects [39]. Advanced SKCM is a difficult disease to treat and requires additional improvement. In the context of ICB therapy and other biological components within the TME, it is vital to have a better knowledge of the immune cell infiltration phenotype and function in order to identify patients who are most likely to respond. Our study developed a method for characterizing PRRS patterns in SKCM by utilizing the TCGA and GEO databases, and the results demonstrated that the PRRS scoring system can be used as an independent and highly predictive prognostic biomarker for patients with SKCM and predicted treatment response to ICB.

This study aimed to determine the function of phagocytosis regulators and their effect on the development of SKCM. We discovered that phagocytosis regulators could influence the number of phagocytes on the one hand, and their expression or mutation, on the other hand, can alter prognosis. We subsequently subtyped the samples according to prognosis-related phagocytosis regulators. We then established a relationship between phagocytosis regulators and survival through survival analysis of molecular subtypes, and discovered disparities in prognosis between subtypes. After that, we identified DEGs between subtypes, performed differential gene subtype identification and functional enrichment analysis, and looked for other differences between phagocytosis-related subtypes. Then, using DEGs between subtypes, we screened for prognostic factors to create a survival model. We established PRRS, a scoring system for predicting survival in patients. We validated the model's efficacy numerous times and coupled pathway analysis, immune infiltration analysis, and mutation analysis to investigate the effects of phagocytosis regulators on SKCM samples. In addition, we probed into potential treatment options using chemotherapy drug response and clinical cohort treatment response and described the model by linking it to known clinical characteristics. Moreover, we used a combination of IHC and qRT-PCR to re-validate expression-based regulators of survival significantly associated with phagocytosis. Our findings suggest: (i) the first use of phagocytosis regulators to assess PRRS patterns in SKCM patients; (ii) a correlation between low PRRS scores and poor prognosis; (iii) a correlation between gene mutations and prognosis in SKCM, and (iv) a correlation between PRRS scores and ICB treatment response.

Recent research has demonstrated that tumor-associated immune cells in the SKCM tumor microenvironment can exert an effect on tumor immune escape and immunosuppression. The TME is composed of tumor cells, immune cells, and stromal cells and has a variety of influences on immunotherapy resistance, metastasis, sensitivity, and medication resistance [40] [41]. Tumor infiltrating

lymphocytes (TILs) such as $CD4^+$ T cells and $CD8^+$ T cells play an essential role in tumor metastasis, recurrence and response rate to immunotherapy [42] [43]. $CD8^+$ T cells exert tumor-killing functions based on cell differentiation and infiltration [44]. Naive $CD8^+$ T cells initiate a differentiation program after infiltration and further differentiate into cytotoxic and effector $CD8^+$ T cells for anti-tumor functions [45]. $CD4^+$ T cells have long been recognized as a critical component of tumor immunotherapy because they are capable of stimulating or suppressing anti-tumor cytotoxic $CD8^+$ T cell responses in secondary lymphoid organs or tumors, hence modulating the tumor immune milieu [46]. Our study revealed that cluster 2 had a more favorable immune activation profile than cluster 1, with significantly higher B cell, $CD4^+$ T cell, and $CD8^+$ T cell cellular content and significantly higher expression of 43 immunological checkpoints. As a result, we expected that individuals in cluster 2 would gain the most benefit from immunotherapy. Cluster 1 had a significantly higher Tumorpurity score than cluster 2, but a significantly lower StormalScore, ImmuneScore, and ESTIMATEScore, implying that cluster 1 is an “immune cold tumor” phenotype associated with a poor prognosis, which can cause tumor cells to evade the immune system, rendering them resistant to immunotherapy. The findings indicate that the gene clusters identified in our study may aid in the creation of more specific immunotherapy. Additionally, our findings imply that pre-existing immune responses are antitumorigenic and positively influence immunotherapy responses [47].

Given the immunological environment’s individual heterogeneity, it is critical to characterize the pattern of immune cell infiltration in individual tumors. As a result, we developed a PRRS scoring method to measure immune cell infiltration patterns using PRRS in order to improve prognosis prediction in patients. Through the TCGA and GEO databases, we validated the PRRS grouping as a strong bio-prognostic marker with improved predictive capacity. We discovered that PRRS scores decreased as pathological stage, tumor stage, and depth of tumor infiltration increased. Further study revealed that PRRS scores for subtype cluster 1 were significantly lower than those for cluster 2, corroborating the notion that low PRRS scores are associated with a bad prognosis. As previously reported [48], high PRRS patients had significantly higher StromalScore, ImmuneScore, and ESTIMATEScore scores than low PRRS patients, while immune infiltrating cell scores were also significantly higher in high PRRS patients than in low PRRS patients, indicating a better prognosis. In addition, by GSEA, we found that genes involved in immunosuppressive pathways such as TGF-β were significantly enriched in the cohort with low PRRS scores. By correlation analysis with cancer hallmarks, we found that immune-related pathways such as innate immune response and adaptive immune response were significantly enriched in the cohort with high PRRS scores. Meanwhile, our investigation discovered that somatic mutations and chromosomal abnormalities are connected with clinical outcomes. We discovered that the frequency of CNV changes was much higher in samples with a low PRRS score than in samples with a high PRRS score, implying a worse prognosis in low PRRS samples. These genes with a high mutation frequency may be prospective targets for future treatment. Based on TCGA-SKCM data, we found that ZDBF2 has the highest mutation rate. Its mutation and methylation are associated with various diseases such as multilocus imprinting disturbances like Temple syndrome (TS14) and Kagami-Ogata syndrome (KOS14) [49], There has also been a reported link between the deletion and Nasopalpebral lipoma-coloboma syndrome, an uncommon

abnormality [50]. RRAGA (Rag A GTPase) mutations, the most often occurring deletion, can have a variety of impacts on lysosomal function and relocalization, cell autophagy, cell proliferation changes, and promoter activity. As important regulators of mTORC1 (mechanistic rapamycin complex 1), mutations are strongly related with autosomal dominant cataracts [51] [52]. Additionally, we evaluated IMvigor210 in immunotherapy patients and discovered that those who achieved clinical remission (CR) due to immunotherapy had significantly higher PRRS scores. Furthermore, we discovered that samples with a high PRRS score were more sensitive to common chemotherapeutic treatment resistance, indicating once again its prognostic value.

In summary, this study elucidated the dysregulation and regulatory significance of phagocytosis regulators in SKCM, established their relationship with tumor heterogeneity, and examined their regulatory patterns in SKCM. This study includes a comprehensive analysis of multiple databases, which points the way forward in terms of the tumor microenvironment, functional analysis, immune response, and drug sensitivity and has significant implications for the development of novel immune drugs and the promotion of immune personalized therapeutic strategies.

Declarations

Ethics approval and consent to participate:

Following permission from the Chinese PLA General Hospital's Human Research Ethics Committee, we collected fifteen pairs of SKCM and para-cancerous normal tissue specimens. Written informed consent was obtained from individual or guardian participants.

Consent for publication

Not applicable.

Availability of data and material

All data generated or analyzed during this study are included in this published article and its supplementary files.

Competing interests

The authors declare that they have no competing interests.

Funding

Not applicable.

Authors' contributions

Jiahua Xing and *Ziqi Jia* wrote the main manuscript text and all the figures, *Yan Li* and *Yan Han* suggested ideas and steps for the article, and participated in the revision of part of the article. All authors read and approved the final manuscript.

Acknowledgements

Not applicable.

References

1. Gordon S. Phagocytosis: An Immunobiologic Process. Immunity. 2016;44:463–75.
2. Arandjelovic S, Ravichandran KS. Phagocytosis of apoptotic cells in homeostasis. Nat Immunol. 2015;16:907–17.
3. Lim JJ, Grinstein S, Roth Z. Diversity and Versatility of Phagocytosis: Roles in Innate Immunity, Tissue Remodeling, and Homeostasis. Front Cell Infect Microbiol. 2017;7:191.
4. Vargas ME, Barres BA. Why is Wallerian degeneration in the CNS so slow? Annu Rev Neurosci. 2007;30:153–79.
5. Chao MP, Alizadeh AA, Tang C, et al. Anti-CD47 antibody synergizes with rituximab to promote phagocytosis and eradicate non-Hodgkin lymphoma. Cell. 2010;142:699–713.
6. Chen J, Zhong MC, Guo H, et al. SLAMF7 is critical for phagocytosis of haematopoietic tumour cells via Mac-1 integrin. Nature. 2017;544:493–7.
7. Ziegenfuss JS, Doherty J, Freeman MR. Distinct molecular pathways mediate glial activation and engulfment of axonal debris after axotomy. Nat Neurosci. 2012;15:979–87.
8. Hong S, Dissing-Olesen L, Stevens B. New insights on the role of microglia in synaptic pruning in health and disease. Curr Opin Neurobiol. 2016;36:128–34.
9. Freeman SA, Grinstein S. Phagocytosis: receptors, signal integration, and the cytoskeleton. Immunol Rev. 2014;262:193–215.
10. Juncadella IJ, Kadl A, Sharma AK, et al. Apoptotic cell clearance by bronchial epithelial cells critically influences airway inflammation. Nature. 2013;493:547–51.
11. Mantovani A, Allavena P, Sica A, et al. Cancer-related inflammation. Nature. 2008;454:436–44.
12. Coussens LM, Zitvogel L, Palucka AK. Neutralizing tumor-promoting chronic inflammation: a magic bullet? Science. 2013;339:286–91.
13. Noy R, Pollard JW. Tumor-associated macrophages: from mechanisms to therapy. Immunity. 2014;41:49–61.
14. Ruffell B, Affara NI, Coussens LM. Differential macrophage programming in the tumor microenvironment. Trends Immunol. 2012;33:119–26.
15. Mantovani A, Marchesi F, Malesci A, et al. Tumour-associated macrophages as treatment targets in oncology. Nat Rev Clin Oncol. 2017;14:399–416.

16. Scott AM, Wolchok JD, Old LJ. Antibody therapy of cancer. Nat Rev Cancer. 2012;12:278–87.
17. Sliwkowski MX, Mellman I. Antibody therapeutics in cancer. Science. 2013;341:1192–8.
18. Weiskopf K, Weissman IL. Macrophages are critical effectors of antibody therapies for cancer. MAbs. 2015;7:303–10.
19. Tsao LC, Crosby EJ, Trotter TN, et al. (2019) CD47 blockade augmentation of trastuzumab antitumor efficacy dependent on antibody-dependent cellular phagocytosis. JCI Insight 4.
20. Morrissey MA, Kern N, Vale RD. CD47 Ligation Repositions the Inhibitory Receptor SIRPA to Suppress Integrin Activation and Phagocytosis. Immunity. 2020;53:290–302.e296.
21. Oldenborg PA, Zheleznyak A, Fang YF, et al. Role of CD47 as a marker of self on red blood cells. Science. 2000;288:2051–4.
22. Haney MS, Bohlen CJ, Morgens DW, et al. Identification of phagocytosis regulators using magnetic genome-wide CRISPR screens. Nat Genet. 2018;50:1716–27.
23. Siegel RL, Miller KD, Fuchs HE, et al. Cancer Statistics, 2021. CA Cancer J Clin. 2021;71:7–33.
24. Ali Z, Yousaf N, Larkin J. Melanoma epidemiology, biology and prognosis. EJC Suppl. 2013;11:81–91.
25. Miller KD, Nogueira L, Mariotto AB, et al. Cancer treatment and survivorship statistics, 2019. CA Cancer J Clin. 2019;69:363–85.
26. Yang L, Xu Y, Yan Y, et al. (2019) Common Nevus and Skin Cutaneous Melanoma: Prognostic Genes Identified by Gene Co-Expression Network Analysis. *Genes (Basel)* 10.
27. Matias M, Pinho JO, Penetra MJ, et al. (2021) The Challenging Melanoma Landscape: From Early Drug Discovery to Clinical Approval. *Cells* 10.
28. Falleni M, Savi F, Tosi D, et al. M1 and M2 macrophages' clinicopathological significance in cutaneous melanoma. Melanoma Res. 2017;27:200–10.
29. Charoentong P, Finotello F, Angelova M, et al. Pan-cancer Immunogenomic Analyses Reveal Genotype-Immunophenotype Relationships and Predictors of Response to Checkpoint Blockade. Cell Rep. 2017;18:248–62.
30. Kamber RA, Nishiga Y, Morton B, et al. Inter-cellular CRISPR screens reveal regulators of cancer cell phagocytosis. Nature. 2021;597:549–54.
31. Huang X, Zhang G, Tang T, et al. Identification of tumor antigens and immune subtypes of pancreatic adenocarcinoma for mRNA vaccine development. Mol Cancer. 2021;20:44.
32. Jozefczuk J, Adjaye J. Quantitative real-time PCR-based analysis of gene expression. Methods Enzymol. 2011;500:99–109.
33. Jenkins RW, Fisher DE. Treatment of Advanced Melanoma in 2020 and Beyond. J Invest Dermatol. 2021;141:23–31.
34. Nakamura K, Okuyama R. Immunotherapy for advanced melanoma: Current knowledge and future directions. J Dermatol Sci. 2016;83:87–94.

35. Leonardi GC, Candido S, Falzone L, et al. Cutaneous melanoma and the immunotherapy revolution (Review). Int J Oncol. 2020;57:609–18.
36. Robert C, Schachter J, Long GV, et al. Pembrolizumab versus Ipilimumab in Advanced Melanoma. N Engl J Med. 2015;372:2521–32.
37. Larkin J, Hodi FS, Wolchok JD. Combined Nivolumab and Ipilimumab or Monotherapy in Untreated Melanoma. N Engl J Med. 2015;373:1270–1.
38. Robert C, Long GV, Brady B, et al. Nivolumab in previously untreated melanoma without BRAF mutation. N Engl J Med. 2015;372:320–30.
39. Wei H, Zhao L, Li W, et al. Combinatorial PD-1 blockade and CD137 activation has therapeutic efficacy in murine cancer models and synergizes with cisplatin. PLoS ONE. 2013;8:e84927.
40. Bian C, Wang Y, Lu Z, et al. (2021) ImmunoAIzer: A Deep Learning-Based Computational Framework to Characterize Cell Distribution and Gene Mutation in Tumor Microenvironment. Cancers (Basel) 13.
41. Landi L, D'Incà F, Gelibter A, et al. Bone metastases and immunotherapy in patients with advanced non-small-cell lung cancer. J Immunother Cancer. 2019;7:316.
42. Vassilakopoulou M, Avgeris M, Velcheti V, et al. Evaluation of PD-L1 Expression and Associated Tumor-Infiltrating Lymphocytes in Laryngeal Squamous Cell Carcinoma. Clin Cancer Res. 2016;22:704–13.
43. Zeng D, Zhou R, Yu Y, et al. Gene expression profiles for a prognostic immunoscore in gastric cancer. Br J Surg. 2018;105:1338–48.
44. Schreiber RD, Old LJ, Smyth MJ. Cancer immunoediting: integrating immunity's roles in cancer suppression and promotion. Science. 2011;331:1565–70.
45. Harty JT, Badovinac VP. Shaping and reshaping CD8 + T-cell memory. Nat Rev Immunol. 2008;8:107–19.
46. Pardoll DM, Topalian SL. The role of CD4 + T cell responses in antitumor immunity. Curr Opin Immunol. 1998;10:588–94.
47. Rooney MS, Shukla SA, Wu CJ, et al. Molecular and genetic properties of tumors associated with local immune cytolytic activity. Cell. 2015;160:48–61.
48. Wang H, Wu X, Chen Y. Stromal-Immune Score-Based Gene Signature: A Prognosis Stratification Tool in Gastric Cancer. Front Oncol. 2019;9:1212.
49. Kagami M, Matsubara K, Nakabayashi K, et al. Genome-wide multilocus imprinting disturbance analysis in Temple syndrome and Kagami-Ogata syndrome. Genet Med. 2017;19:476–82.
50. Chacón-Camacho OF, Sobreira N, You J, et al. Exome sequencing identifies a de novo frameshift mutation in the imprinted gene ZDBF2 in a sporadic patient with Nasopalpebral Lipoma-coloboma syndrome. Am J Med Genet A. 2016;170:1934–7.
51. Chen JH, Huang C, Zhang B, et al. Mutations of RagA GTPase in mTORC1 Pathway Are Associated with Autosomal Dominant Cataracts. PLoS Genet. 2016;12:e1006090.

52. Zhang H, Yan S, Khambu B, et al. Dynamic MTORC1-TFEB feedback signaling regulates hepatic autophagy, steatosis and liver injury in long-term nutrient oversupply. Autophagy. 2018;14:1779–95.

Figures

Figure 2

Phagocytosis modulators regulate the involvement of macrophages in tumor development. (A-L) Phagocytosis modulators regulate macrophage phagocytosis. (A-F) Top six Pearson correlations of phagocytosis modulators with macrophage enrichment scores are shown. (G-L) Demonstration of differences in macrophage enrichment scores in high and low gene expression groups (*P<0.05, **P <0.01, ***P <0.001, ****P <0.0001). (M-P) Functional analysis of phagocytosis regulatory factors. (M) Functional analysis of biological process. (N) Functional analysis of cellular component. (O) Functional analysis of molecular function. (P) Functional analysis of KEGG. (Q-S) Abnormal phagocytosis in tumors. (Q) WP microglia pathogen phagocytosis pathway of significant enrichment results for stage III-IV subgroup samples. (R) HP hemophagocytosis of significant enrichment results for stage III-IV subgroup samples. (S) GOBP phagocytosis recognition of significant enrichment results for stage III-IV subgroup samples.

Figure 3

Transcriptional and genetic alterations of phagocytosis regulators in tumors. (A-H) Differential expression of phagocytosis regulatory factors in cancer samples across clinical factors, including age, gender, pathologic M, pathologic N, pathologic T, tumor stage, breslow depth, clark level. (I-L) Genomic alterations in the regulators of phagocytosis. (I) Mutation profile of the top 20 phagocytosis regulators. (J) Sample mutation frequency display. (K) Copy number change frequency statistics of the top 30 phagocytosis regulators. (L) The positions of all phagocytosis regulators on each chromosome are shown.

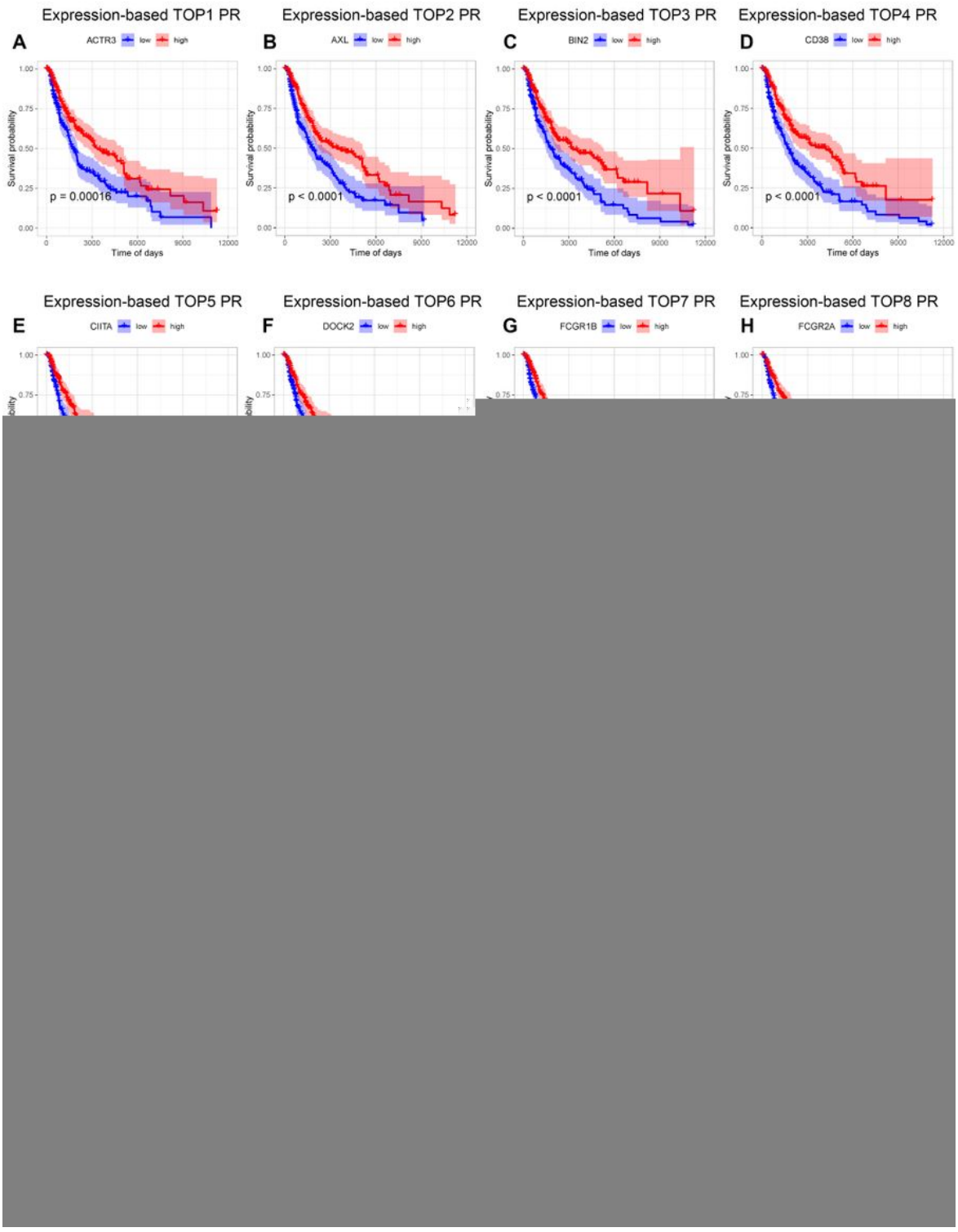

Figure 4

Effect of phagocytosis regulators on tumor survival. (A-I) Display of Kaplan-Meier curves of the top nine expression-based regulators of survival significantly associated with phagocytosis, including ACTR3, AXL, BIN2, CD38, CIITA, DOCK2, FCGR1B, FCGR2A, FCRL3. (J-P) Demonstration of Kaplan-Meier curves for mutation-based regulators of survival significantly associated with phagocytosis, including CADM1, RAC1, PTPRC, CIITA, TMEM119, UBR4, ANAPC7.

Figure 5

Different modes of phagocytosis regulation in tumors. (A-F) Identification of molecular isoforms of phagocytosis regulators. (A) Heat map of unsupervised clustering of samples. (B) Cumulative distribution graph. (C) Unsupervised clustering gravel map. (D) Inter-subtype Overall survival (OS)-based Kaplan-Meier curves. (E) Principal component analysis (PCA) scatter plot. (F) Heat map of phagocytosis regulatory factor expression. (G) Heat map display of enrichment analysis results of the inter-subtype hallmark pathway (*P<0.05, **P <0.01, ***P <0.001, ****P <0.0001). (H-L) Differences in immune infiltrating cells between subtypes. (H) Immunization score difference display of ImmuneScore. (I) Immunization score difference display of StromalScore. (J) Immunization score difference display of ESTIMATEScore. (K) Immunization score difference display of TumorPurity. (L) Differences in immuno-infiltrating cell enrichment scores are shown (*P<0.05, **P <0.01, ***P <0.001, ****P <0.0001). (M) Differences in immune checkpoint expression between subtypes (*P<0.05, **P <0.01, ***P <0.001, ****P <0.0001).

Figure 6

Validation of regulatory mechanisms among different phagocytosis isoforms. (A-D) Functional enrichment analysis of differentially expressed genes. (A) Functional analysis of biological process. (B) Functional analysis of cellular component. (C) Functional analysis of molecular function. (D) Functional analysis of KEGG. (E-F) Unsupervised clustering based on differential genes. (E) Heat map display of differential gene expression. (F) Display of Kaplan-Meier curves between differential genetic subtypes. (G) Heat map display of expression of phagocytosis regulatory factors among differential genetic isoforms.

Figure 7

Phagocytosis regulators related system (PRRS) construction. (A-E) Model effectiveness validation of PRRS for TCGA data. (A) Build model Kaplan-Meier curve validation. (B) Receiver operating characteristic (ROC) curve validation. (C) PRRS score graphs for all samples. (D) Scatter plot of survival time for all samples. (E) Heat map of gene expression in the model. (F-J) Model effectiveness validation of PRRS for GSE54467 data. (F) Build model Kaplan-Meier curve validation. (G) ROC curve validation. (H) PRRS score graphs for all samples. (I) Scatter plot of survival time for all samples. (J) Heat map of gene expression in the model.

Figure 8

PRRS correlates with tumor prognosis and clinical features. (A-B) TCGA SKCM data to verify whether PRRS grouping is an independent prognostic factor. (A) TCGA SKCM univariate cox regression analysis. (B) TCGA SKCM multivariate cox regression analysis. (C-D) GSE54467 data to verify whether PRRS grouping is an independent prognostic factor. (C) TCGA SKCM univariate cox regression analysis. (D) TCGA SKCM multivariate cox regression analysis. (E) Differences in PRRS in clinical characteristic groupings (ns, not significant, *P<0.05, **P<0.01, ***P<0.001, ****P<0.0001).

Figure 9

Analysis of the molecular mechanisms of different PRRS. (A) PRRS and hallmarks correlation display (*P<0.05, **P<0.01, ***P<0.001). (B-C) Functional differences between PRRS subgroups. (B) Display of GO function enrichment results for PRRS grouping. (C) Display of KEGG function enrichment results for PRRS grouping. (D-H) Different PRRS grouping TME (ns, not significant, *P<0.05, **P<0.01, ***P<0.001, ****P<0.0001). (D) Differences of ImmuneScore in immune infiltrating cells between high and low PRRS subgroups. (E) Differences of ESTIMATEScore in immune infiltrating cells between high and low PRRS subgroups. (F) Differences of StromalScore in immune infiltrating cells between high and low PRRS subgroups. (G) Differences of TumorPurity in immune infiltrating cells between high and low PRRS subgroups. (H) Differences in immune infiltrating cell enrichment scores between high and low PRRS subgroups were demonstrated. (I-K) Demonstration of genetic CNV among PRRS subgroups. (I) Presentation of individuals in CNV of high PRRS samples. (J) Presentation of individuals in CNV of low PRRS samples. (K) CNV frequency statistics between the two groups. (L-M) Demonstration of gene mutations among PRRS subgroups. (L) Mutation display of high PRRS samples. (M) Mutation display of low PRRS samples.

Figure 10

Potential treatment strategies for PRRS. (A-F) Prediction of drug resistance to different chemotherapeutic agents in samples from high and low risk groups, including Etoposide, Bleomycin, Lenalidomide, Bexarotene, Midostaurin, Embelin. (ns, not significant, *P<0.05, **P<0.01, ***P<0.001, ****P<0.0001). (G-K) Risk model validation of IMvigor 210 data. (G) Kaplan-Meier curves for high and low PRRS groups. (H) AUC time-dependent receiver operating characteristic (ROC) curves. (I) Statistics on the distribution of PRRS scores in each immune effect classification. (J) Distribution statistics of immunotherapy response in high and low PRRS groups. (K) Bar chart display of PRRS subline score for different response type samples. (L) Tumor-intrinsic mechanisms and their effect on the antitumor immune response.

Figure 11

Validation of the mRNA and protein expression of expression-based regulators of survival significantly associated with phagocytosis. Results of the first column represents the immunohistochemistry (IHC) images of the normal skin obtained from the Human Protein Atlas (100 um). Results of the second column represents the IHC images of skin cutaneous melanoma obtained from the Human Protein Atlas (100 um). Results of the third column represents the semiquantitative analysis results which derived from the first two columns. Results of the forth column represents the qRT-PCR results from four cell lines (Hacat, PIG1, A375 and SK-MEL 14). Results of the fifth column represents the qRT-PCR results of tissue specimens from 15 patients, which taken from normal skin and skin cutaneous melanoma. (A-I) represents the results of nine expression-based regulators of survival significantly associated with phagocytosis, including ACTR3, AXL, BIN2, CD38, CIITA, DOCK2, FCGR2A, FCRL3, FCGR1B (ns, not significant, *P<0.05, **P <0.01, ***P <0.001, ****P <0.0001).

Supplementary Files

This is a list of supplementary files associated with this preprint. Click to download.

- SupplementaryFigure1.jpg
- SupplementaryFigure2.jpg
- SupplementaryFigure3.jpg
- SupplementaryTable.docx